Optimization of sub-Doppler DAVLL on the rubidium D2 line

M L Harris, S L Cornish, A Tripathi and I G Hughes

Department of Physics, Durham University, South Road, Durham, DH1 3LE, UK

E-mail: i.g.hughes@durham.ac.uk

Abstract. We discuss the physics of sub-Doppler DAVLL spectroscopy, which employs a pump beams with an axial magnetic field to induce dichroism in an atomic vapour. The dichroism is measured by a counterpropagating probe beam, while the pump generates sub-Doppler spectral features. The magnitude of the field is chosen to shift the frequency of the absorption features by an amount comparable to their linewidth. The reference signals obtained are ideal for laser frequency discriminant signals (laser 'locking' to the atomic transition) without frequency modulation. We discuss the sensitivity of the spectra to magnetic field, laser power, and polarization purity, and suggest operating parameters for the ^{87}Rb $F = 2 \rightarrow F^{'} = 3, 2$ crossover transition which maximise the signal amplitude and gradient.

PACS numbers: 32.60.+i, 33.55.Ad, 42.62.Fi

1. Introduction

Many atomic physics experiments use diode lasers which require active stabilization, or 'locking', of their frequency. For example, diode lasers are used extensively in the field of laser cooling and trapping [1], where control of the laser frequency to a fraction of the linewidth of the atomic transition (~ 1 MHz) is required. A frequently-used scheme involves 'dithering' [2] the laser frequency to obtain a signal (the 'error signal') which can be used to lock the laser to an atomic reference. Such a system employs frequency modulation of the laser and subsequent lock-in detection, yielding steep gradients in the error signals and zero-crossings coincident with atomic reference transitions. It is also possible to perform frequency-modulation spectroscopy using an external phase modulator driven at radio frequencies [3]. In some applications, however, it is advantageous to avoid frequency modulation of the laser. Many dither-free techniques for producing a suitable error signal have been developed, including polarization spectroscopy [4], dichroic atomic vapour laser locking (DAVLL) [5], a combination of saturated absorption and DAVLL [6, 7], Sagnac interferometry [8], prismatic deflection [9], using acousto-optic modulators [10], low-field Faraday polarimetry [11], velocity-selective saturated absorption spectroscopy [12] and bi-polarization spectroscopy [13].

The performance and capabilities of these locking techniques differ. There are tradeoffs between simplicity, cost, ease of operation, location of zero-crossings with respect to the atomic reference, sensitivity to external perturbations, and the frequency deviation the system can tolerate and still return to the desired lock-point ('capture range'). In conventional DAVLL, a single probe beam produces Doppler-broadened spectral features, yielding an error signal with a wide capture range (~ 0.5 GHz for alkali metal atoms at room temperature). Sub-Doppler resolution can be achieved by combining saturated absorption and DAVLL in a pump-probe scheme. The resulting error signal has a steep gradient through the zero-crossings. The capture range of this method (hereafter referred to as sub-Doppler DAVLL) is typically tens of MHz. The presence of zero-crossings associated with six atomic references eliminates a major drawback of DAVLL, namely that the error signal is prone to long term drifts, necessitating periodic adjustments to the lock point.

The aim of this work is to provide a detailed experimental study of the error signal lineshapes arising from sub-Doppler DAVLL spectra of the D2 transitions in ^{85}Rb and ^{87}Rb. We have characterised the dependence of the error signal's amplitude and gradient on the magnetic field and the pump beam power. We also discuss the role of polarization purity in generating the lineshapes. We have not included measurements of the long-term frequency stability of a laser locked using this scheme, as this will depend strongly on environmental effects, the laser used, and the details of the servo-loop design. We focus instead on describing the physics of the sub-Doppler DAVLL process, and the features which determine the amplitude and slope of the lock signals, as these are likely to be universally applicable in other laboratories. The structure of the paper is as follows: Section 2 summarises the principles of sub-Doppler DAVLL; Section 3

describes the experimental apparatus and details of the methodology; Section 4 presents and discusses the results, and we draw our conclusions in Section 5.

2. Principles of Sub-Doppler DAVLL Spectroscopy

It is possible to resolve excited state hyperfine structure in the D2 lines of alkali metal atoms with a simple pump-probe setup, using counterpropagating beams of the same frequency. The presence of the pump beam reduces the number of ground-state atoms with which the probe can interact via the processes of saturated absorption and hyperfine pumping [14]. Sub-Doppler resolution is achieved because only atoms with a small longitudinal velocity (those with a Doppler shift comparable to or less than the natural linewidth) interact with both pump and probe beams. Naively, one might expect three resonances owing to the $\Delta F = 0, \pm 1$ selection rule; however, crossover resonances are also observed at frequencies halfway between conventional resonances [14].

In the DAVLL technique, a linearly polarized probe beam is incident on an atomic vapor with the wavevector of the light parallel to the axis of an applied magnetic field. After interacting with the atoms, the probe passes through a quarter wave plate before impinging on a polarizing beamsplitter (PBS). The linearly polarized beam can be decomposed into two orthogonal circularly polarized beams of equal amplitude. The signals measured by detectors placed in the output arms of the PBS are proportional to the intensity of the right and left circularly polarized beams. In the absence of a magnetic field, different m_F states are degenerate and the σ^+ and σ^- transitions overlap. When a finite magnetic field is applied, the degeneracy is lifted and the medium becomes dichroic: the centre frequencies of the σ^+ and σ^- absorption lines are displaced in different directions. The magnetic field magnitude is chosen such that the frequency displacement of the absorption lines is similar to their Doppler-broadened widths. Consequently, the difference signal has a dispersion-like shape, with a zero-crossing at line centre and a wide capture range.

Sub-Doppler DAVLL [6, 7] is a hybrid of the two techniques described above. The linearly polarized probe beam is analysed after passing through the atomic vapor cell, and sub-Doppler features are induced by a counterpropagating pump beam. Although saturated absorption/hyperfine pumping spectra have been observed for decades, providing a full theoretical description is still a topic of active study [15]. A complete description of sub-Doppler DAVLL would also have to include the magnetic field applied to induce dichroism. We do not present such a theory for the spectra in this work; instead, we focus on explaining the choice of parameters which optimise the empirically observed sub-Doppler DAVLL spectra, and offer comparisons to polarization spectroscopy.

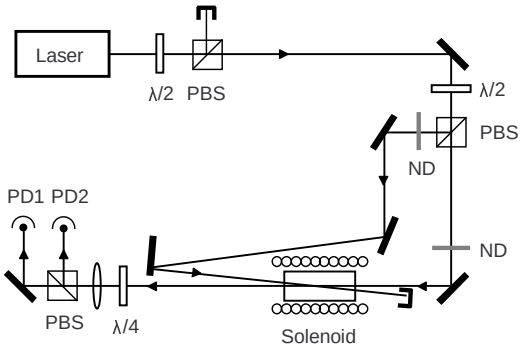

Figure 1. Optical layout used for sub-Doppler DAVLL spectroscopy. The pump and probe beams are separated by a polarising beamsplitter (PBS). Neutral density filters (ND) are used with PBSs and half wave plates ($\lambda/2$) to regulate the intensities of each beam independently. Additional PBSs and half wave plates (not shown) are placed in the pump and probe beams to 'clean up' the polarization. The cell containing room-temperature rubidium vapor is located inside a solenoid. The crossing angle between the pump and probe beams inside the cell has been exaggerated for clarity. Two detectors (PD1 and PD2) monitor the absorption of light which has driven σ^+ and σ^- transitions.

3. Experimental Details

The experimental setup (Fig. 1) uses a grating-stabilised diode laser (Toptica DL100) to provide light at 780 nm. After the laser, a low order half wave plate (Casix WPL1210) is used in conjunction with a polarising beamsplitter (Casix PBS0201) to transmit a fraction of the laser light ($\sim$ 5 mW) into the spectroscopy setup. An isolator prevents light from being reflected back into the laser. Neutral density filters are used to vary the pump and probe powers independently. At the vapor cell the probe beam has a $1/e^2$ radius of (0.84$\pm$0.05) mm horizontally and (0.81$\pm$0.02) mm vertically.

The pump and probe beam are counterpropagated along a 7 cm long vapor cell, with a crossing angle of 9 mrad between the two beams. This small angle can be eliminated entirely by using a nonpolarising beamsplitter to overlap the beams; note, however, that many inexpensive beamsplitters are highly birefringent. After the cell the probe beam passes through a low-order quarter wave plate (Casix WPL1210) followed by another polarizing beamsplitter (PBS). Simple amplified photodiode circuits in the output arms of the PBS are used to monitor the absorption of the σ^+ and σ^- transitions. Both detectors were calibrated and checked for linearity of response with respect to input power. The detectors have a measured responsivity of (0.45$\pm$0.04) AW^{-1}, and the amplifiers a transimpedence of 5.3 MΩ.

The vapor cell was placed in a 7 cm long solenoid with 22 turns per cm; this generated a longitudinal field of (23.15$\pm$0.08) GA^{-1}. Saturated absorption/hyperfine pumping spectroscopy [14] was employed to calibrate the frequency of the sub-Doppler DAVLL spectra using the known Rb hyperfine splittings [16].

4. Results and Discussion

Figure 2 (a) shows typical sub-Doppler spectra of the $F = 2 \rightarrow F'$ transitions in ^{87}Rb and $F = 3 \rightarrow F'$ transitions in ^{85}Rb recorded with a magnetic field of 9.5 G. The conventional DAVLL spectrum, with features of the order of ~ 0.5 GHz wide, is seen as a background. As the widths of the sub-Doppler features are more than an order of magnitude narrower than the Doppler-broadened absorption lines, the field needed is correspondingly weaker than the field of ~ 140 G which gives the optimal conventional DAVLL signal [5]. Figure 2 (b) shows the ^{87}Rb $F = 2 \rightarrow F'$ transitions in greater detail. The anti-symmetric dispersion-like nature of the sub-Doppler features is evident. Six features are seen, one for each sub-Doppler transmission peak. The steepest gradients of the sub-Doppler DAVLL peaks are approximately coincident with the centre frequencies of the Rb hyperfine transitions (crossover resonances), as indicated by the solid (dashed) lines in Figure 2 (b). Note that the strongest locking signals are obtained for the transitions which show the largest sub-Doppler transmission features.

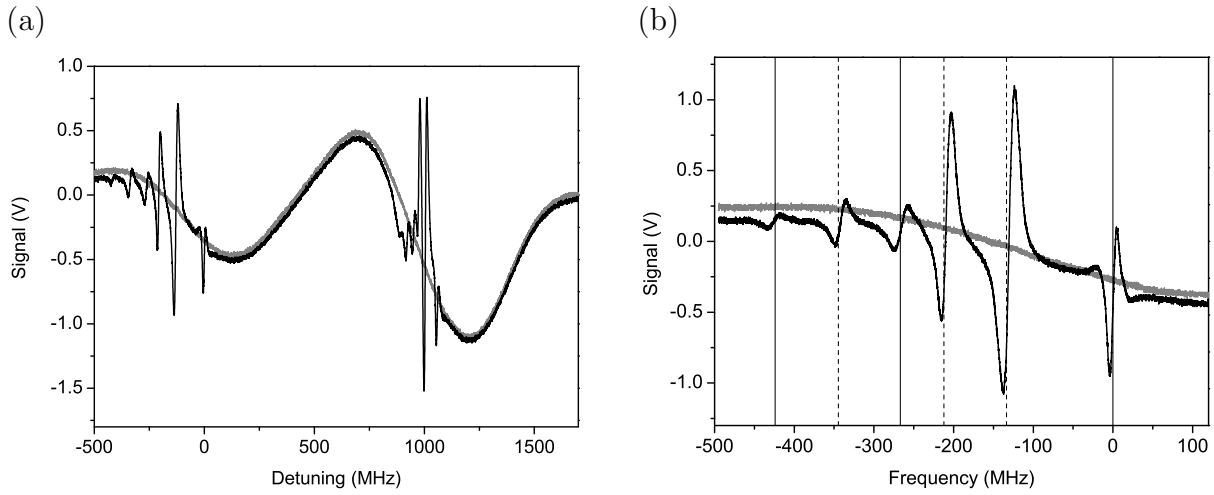

Figure 2. (a) Typical sub-Doppler DAVLL spectra recorded for the $F = 2 \rightarrow F'$ line in ^{87}Rb and $F = 3 \rightarrow F'$ ^{85}Rb (black line). The sub-Doppler features are superimposed on the conventional DAVLL signal (grey line) obtained by blocking the pump beam. (b) A zoomed-in section of (a) showing the sub-Doppler DAVLL signal for the $F = 2 \rightarrow F'$ transitions of ^{87}Rb. Vertical lines indicate the expected line centres of the three transitions (solid lines) and three crossovers (dashed lines). Small discrepancies in the location of spectral features relative to the line centres arise from the slightly nonlinear laser scan. Spectra were taken at a magnetic field of 9.5 G, a pump power of 154 μW, and a probe power of 20 μW.

4.1. Dependence of sub-Doppler DAVLL spectra on pump power and magnetic field

Changing the magnetic field and the pump power produces marked differences in the sub-Doppler DAVLL lineshapes. The dependence of the properties of interest for locking

(the peak to peak amplitude and the gradient of the signal at the zero crossing) were quantified for the $F = 2 \rightarrow F' = 2, 3$ crossover transition in ^{87}Rb. This feature was selected because it is among the strongest lines in all four Rb transitions, and is separated from other spectral features by many tens of MHz. Other transitions are discussed briefly in Section 4.3.

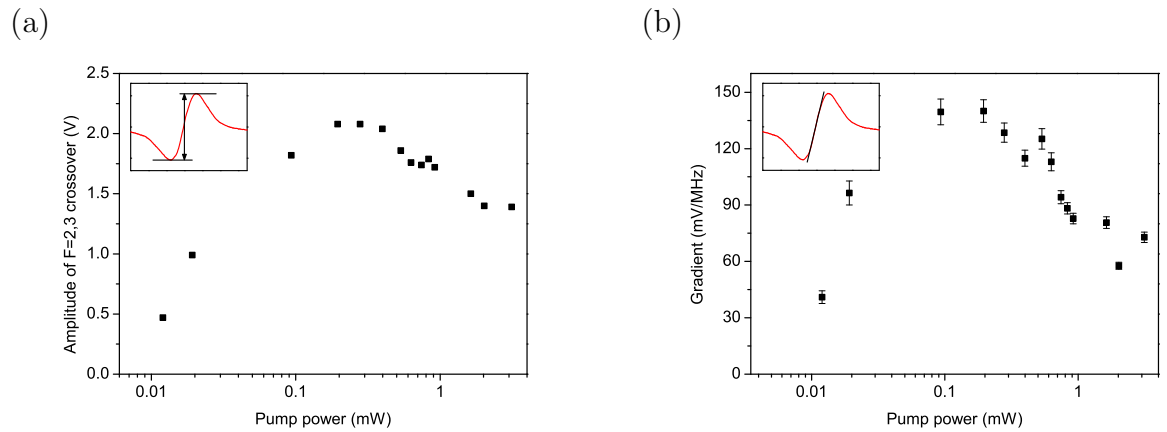

Figure 3. Dependence of (a) amplitude and (b) gradient on pump power for the ^{87}Rb $F = 2 \rightarrow F' = 2, 3$ crossover transition feature. The data were taken with a probe power of 20 μW and a magnetic field of 9.5 G. Error bars represent measurement uncertainties; the frequency calibration produces an additional systematic uncertainty of 3% in the magnitude of the gradient.

Figure 3 shows the evolution of (a) the amplitude and (b) the line-centre gradient of the $F = 2 \rightarrow F' = 2, 3$ crossover transition in ^{87}Rb as a function of pump power for a fixed magnetic field of 9.5 G. Both the amplitude and gradient are maximised for pump powers of $150-300$ μW, with the gradient reduced significantly due to power broadening above 700 μW. The probe power was fixed at 20 μW. The choice of probe power is a trade-off between two effects. A higher probe power gives a better signal-to-noise ratio from the photodiode circuit. However, a low probe beam power ensures that one is in the weak-field limit, for which the absorption is largest [14].

Figure 4 shows the effect of the solenoid's magnetic field on (a) the amplitude and (b) the gradient for three pump powers. The amplitude increases monotonically for all three pump powers up to a field of 20 G, at which point it begins to level off or decrease for the two lower pump powers. The gradient reaches its maximum value of 150 mV MHz^{-1} with an optimised pump power of 154 μW for magnetic fields between $10-15$ G. A reduction in gradient is expected for larger fields because the Zeeman shift is such that the σ^+ and σ^- transitions differ in frequency by more than one natural linewidth. Above $\sim$ 30 G the smoothness of the sub-Doppler DAVLL lineshape is also compromised as Zeeman splitting begins to appear in the hyperfine structure.

Another relevant quantity for locking a laser's frequency to an atomic transition is the magnitude of the difference between the transition frequency and the zero-crossing of

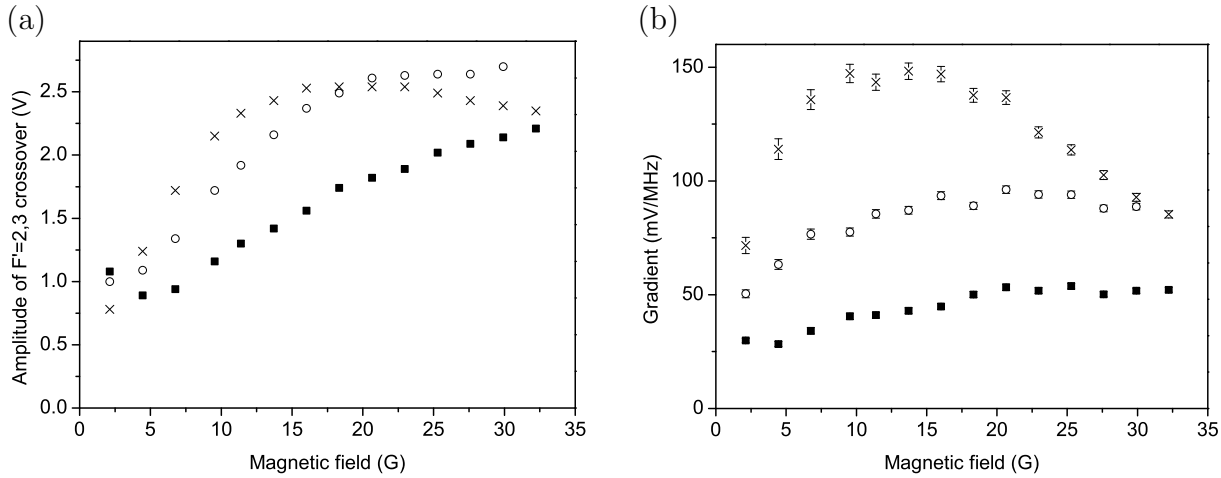

Figure 4. Dependence of (a) amplitude and (b) gradient of the $F = 2 \rightarrow F^{'} = 2, 3$ crossover transition in ^{87}Rb on magnetic field. The data were taken with a probe power of 20 μW and pump powers of 154 μW (crosses), 784 μW (circles) and 3.04 mW (squares).

the error signal. These zero-crossing shifts were measured by turning down the laser scan and comparing the zero-crossing frequency to the frequency of the associated saturated absorption peak. Measurements of the zero-crossing shift as a function of magnetic field showed that for fields between $5 - 20$ G, the magnetic field dependence of the zero crossing frequency is less than (70±20) kHzG^{-1}. A field-independent frequency offset of between (0.6 ± 0.2) and (4.2 ± 0.2) MHz was observed for the different zero-crossing angles discussed in Section 4.4. These offsets are related to the slope of the background DAVLL signal, and can be set to any value within the capture range of the error signal by fine adjustments to the quarter wave plate angle.

The settings of magnetic field and pump power which maximise signal gradient and amplitude have clear trends. Empirically, one increases the pump power for a (low) fixed magnetic field until the gradient starts to decrease, then increases the field to produce the largest peak-to-peak amplitude without compromising the gradient. As these optimal field and power settings are largely uncorrelated, a few loops of the above procedure rapidly produces a reliable lock-point.

4.2. Comparison of sub-Doppler DAVLL and polarization spectroscopy

The optical setup required to generate sub-Doppler DAVLL is very similar to that required for polarization spectroscopy. In the latter, the quarter wave plate is moved from the probe to the pump beam to produce a circularly polarized pump beam. An additional half wave plate is placed in the probe beam before the vapor cell to set the error signal to zero with the pump beam blocked. Sub-Doppler DAVLL requires a solenoid, whereas to maximise the polarization spectroscopy signal a magnetic shield is often used. A shield was not used here because the ambient magnetic field was

largely directed along the cell axis; consequently, spectra appeared very similar with and without a shield present. For other experiments in our group, the ambient magnetic field direction is at an angle relative to the cell, and use of a shield can increase the magnitude of the polarization spectra features by up to a factor of two.

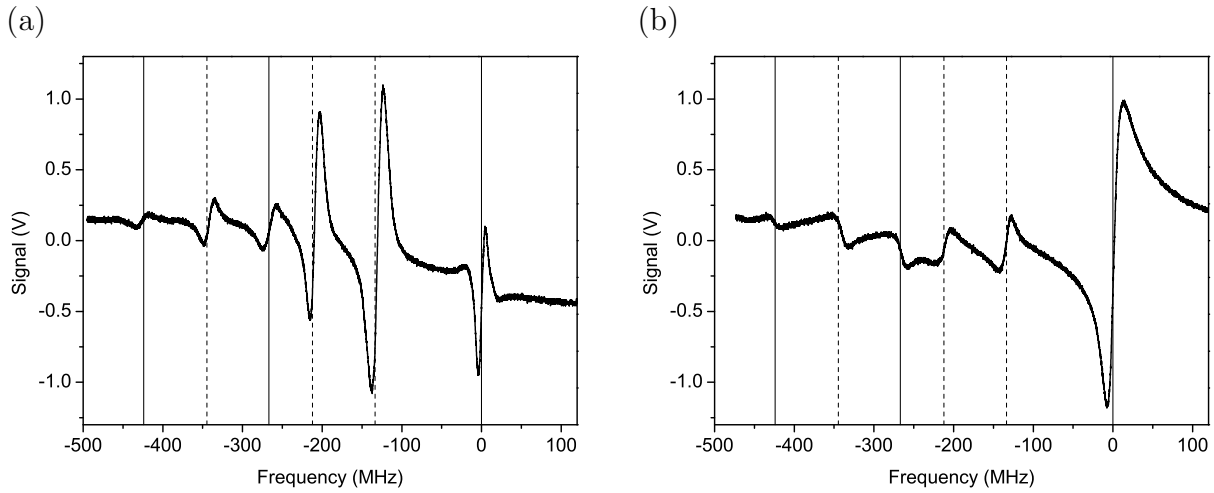

Figure 5. Comparison of (a) sub-Doppler DAVLL with (b) polarization spectroscopy of the $F = 2 \rightarrow F'$ transitions in ^{87}Rb. The data were taken with the same photodiode detectors at a pump (probe) power of 154 μW (20 μW) The magnetic field was 9.5 G for the sub-Doppler DAVLL spectra and < 0.3 G for the polarization spectra.

Figure 5 shows a comparison of polarization and sub-Doppler DAVLL spectra for the ^{87}Rb $F = 2 \rightarrow F'$ transitions. The most noteworthy feature is the difference in amplitudes of spectral features arising from the same transitions. Polarization spectroscopy relies on atoms in the medium absorbing many photons from the circularly polarized pump beam to drive the population towards a maximal m_F state, thus it is hampered by the process of hyperfine pumping. Consequently the closed transition $F = 2 \rightarrow F' = 3$ dominates [17]. In contrast, the crossover peaks involving open transitions are enhanced significantly by hyperfine pumping [14], thus the sub-Doppler DAVLL spectra for these peaks are correspondingly larger. The choice of which technique to use essentially comes down to the question of whether an error signal centred on the closed transition, or one displaced from the closed transition by an excited state hyperfine interval, is desired. This depends on the exact spectroscopic application, and the availability of acousto-optic modulators to modify the frequency of the beam used in an experiment with respect to the beam used in the spectroscopy setup. Note also that for certain atomic transitions, *e.g.* the $^1S_0 \rightarrow ^1P_1$ transition in ^{88}Sr, polarization spectra do not exist, whereas sub-Doppler DAVLL spectra can still be generated.

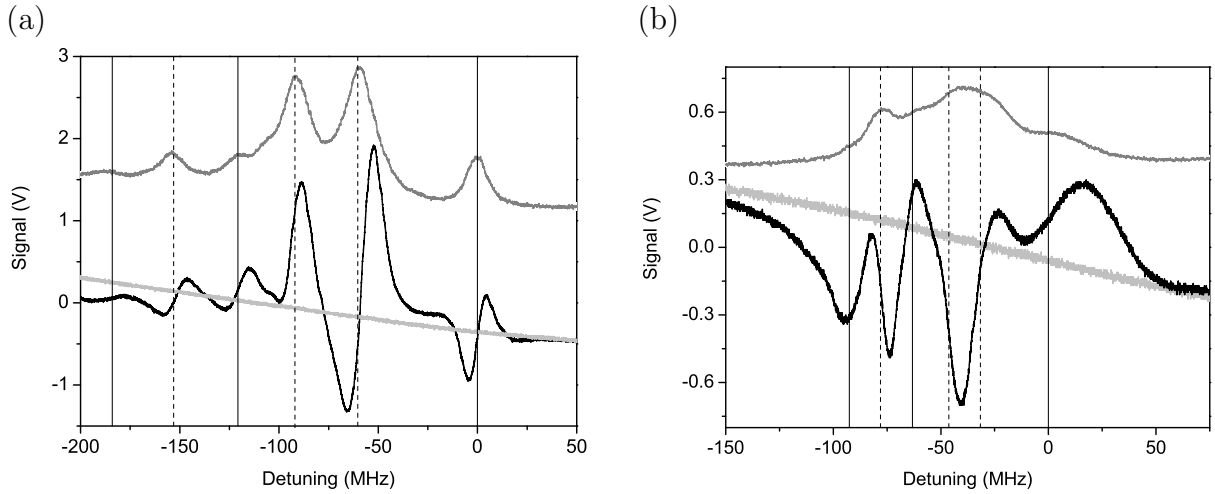

Figure 6. Sub-Doppler DAVLL signal for the (a) $F = 3 \rightarrow F^{'}$ and (b) $F = 2 \rightarrow F^{'}$ transitions of ^{85}Rb. The small hyperfine splitting of the latter transitions make it difficult to distinguish individual features. Light grey lines show the signal without the pump beam. Dark grey lines show the saturated absorption/hyperfine pumping spectra, which have been offset for clarity. The magnetic field and beam powers are the same as in Figure 5.

4.3. Sub-Doppler DAVLL spectra of other Rb transitions

The sub-Doppler DAVLL spectra of other Rb transitions also provide useable error signals for laser locking. Figure 6 (a) shows the ^{85}Rb $F = 3 \rightarrow F^{'}$ transitions. The $F' = 3, 4$ crossover feature appears particularly favourable for locking, with a well-defined zero crossing despite being separated from other features by only a few tens of MHz.

The sub-Doppler DAVLL spectra for the ^{85}Rb $F = 2 \rightarrow F^{'}$ transitions (Figure 6 (b)) share a feature with polarization spectroscopy on the same transitions [17]: namely, the hyperfine splitting is so small that the six distinct spectral features seen on the other transitions partially overlap. The zero-crossings are thus both sensitive to the parameters chosen and not trivially related to the atomic reference transitions. It is possible to produce a zero-crossing for this transition with a greater amplitude and steeper gradient by deliberately power-broadening the sub-Doppler features. The magnetic field plays little role under these conditions. The resulting spectra appear very similar to power-broadened saturated absorption/hyperfine pumping spectra of the same transition, which can also be used in a 'side of peak' locking technique.

For the ^{87}Rb $F = 1 \rightarrow F^{'}$ transitions, the hyperfine splitting is larger, and the sub-Doppler features more distinct. However, the fraction of light absorbed in a 7 cm vapor cell for this transition is less than 10% at room temperature, and the amplitude of the largest crossover feature is approximately five times smaller than the ^{85}Rb $F = 3 \rightarrow F' = 3, 4$ and ^{87}Rb $F = 2 \rightarrow F' = 2, 3$ features. Ohmic heating from a specially-designed solenoid has been used to increase absorption and improve the

conventional DAVLL signal for this transition [18]. This technique could be extended to sub-Doppler DAVLL by using a double solenoid, in which opposing currents generate a net magnetic field of 10 G along the axis of the vapor cell whilst also heating it to > 50 °C.

4.4. Dependence of sub-Doppler DAVLL lineshapes on polarization purity

Changing the angle of the quarter wave plate influences the shape of both the conventional DAVLL background [5] and the sub-Doppler DAVLL signals. For all spectra presented here, the wave plate angle was chosen such that the signal is zero far from resonance. In a system where the pump and probe beams are exactly linearly polarized and all polarization optics are perfect, such 'zero-crossing angles' will be observed whenever one of the axes of the quarter wave plate is aligned at an angle of 45 degrees relative to the probe beam's polarization angle (horizontal). Rotating the quarter wave plate through 360 degrees will therefore produce four zero-crossing angles located 90 degrees apart. The sub-Doppler DAVLL spectra obtained at successive zero-crossing angles will be identical except for a sign change, and equally well-suited for laser locking.

The optical setup shown in Figure 1 was designed to produce polarization purities of better than 300:1 in both beams. We have found that whenever PBSs are used in conjunction with half wave plates to produce a low-power beam, *e.g.* for spectroscopy, the polarization purity of the weaker output beam is compromised. This is because a PBS typically allows a small fraction of input light with the wrong polarization to 'leak' into each arm of the beamsplitter. If the power in the weaker output beam is comparable to this 'leaked' power, the polarization of the beam will be highly elliptical (impure). To improve the polarization purity of the spectroscopy beams, additional PBSs and half wave plates (not shown in diagram) were inserted in the pump and probe beams after the beams are separated. This method is very effective at 'cleaning up' the polarization of the light transmitted through the PBSs; the polarization purity of the pump and probe beams was $> 350 : 1$ at the cell compared to 70:1 immediately after the separating PBS.

Ultimately, however, the behaviour of the sub-Doppler DAVLL signal is strongly affected by the PBS used as an analyser. The fractional leakage noted above is slightly higher for the PBS's rejected arm, and this small anisotropy affects both the number of zero-crossing angles and the interval between them. To understand this behaviour, we modelled the PBS and quarter wave plate using a Jones matrix approach [19]. Based on the measured amounts of vertically and horizontally polarized light in each arm of the analyser, the model predicts *pairs* of zero-crossing angles separated by (10 ± 2) degrees. Experimentally, we observed zero-crossing angles whenever an axis of the quarter wave plate was aligned at 40 or 50 degrees relative to the probe beam polarization angle, in excellent agreement with the model. Figure 7 (a) shows the sub-Doppler DAVLL spectra obtained for two such zero-crossing angles. The sub-Doppler features are nearly

identical, but the peaks in the Doppler background (inset) are separated by $\sim$ 200 MHz. This leads to a difference of (1.7 ± 0.1) MHz between the two angles in the frequency of the zero-crossing associated with the $F = 2 \rightarrow F' = 2, 3$ crossover feature.

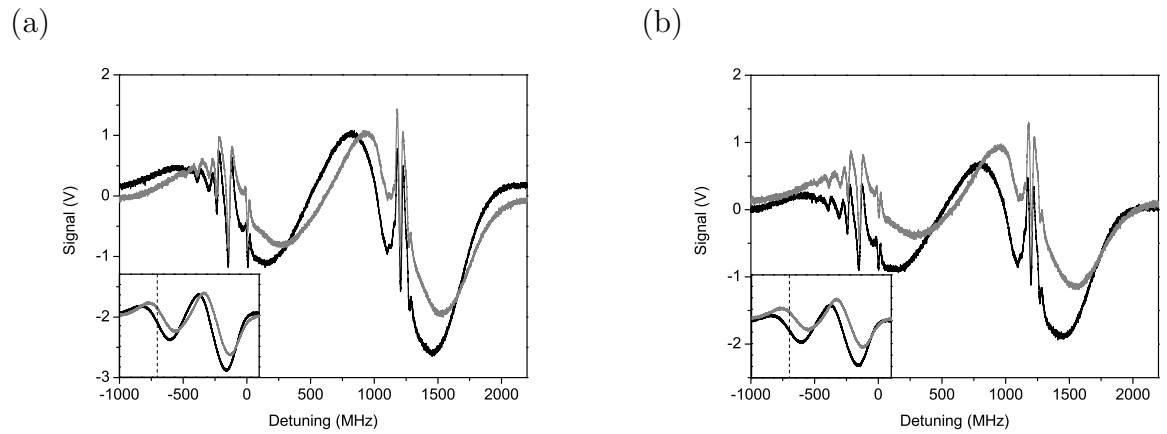

Figure 7. Sub-Doppler DAVLL spectra of the $F = 2 \rightarrow F^{'}$ ($F = 3 \rightarrow F^{'}$) transitions in ^{87}Rb (^{85}Rb). Spectra from successive zero-crossing angles are indicated with grey and black lines. Insets show the background DAVLL signal obtained with the pump beam blocked. A dashed line indicates the location of the crossover feature studied in Section 4.1. (a) Spectra obtained with a polarization purity of $> 350 : 1$ in the pump and probe beams. Small changes in the position of the sub-Doppler features relative to the Doppler background have little effect on their suitability for use in laser locking. (b) Reducing the polarization purity to 145:1 produces larger offsets, increasing the sensitivity of the error signal to changes in polarization or magnetic field.

The magnitude of these shifts and the separation between each zero crossing angle in a pair (ideally zero) are measures of polarization quality. Figure 7 (b) shows sub-Doppler spectra obtained when the polarization purity of the probe and pump beams was deliberately reduced to 145:1. With the polarization purity halved, the separation of the zero-crossing angles increased to 18 degrees. Although the sub-Doppler spectra appear qualitatively similar for the two angles, the peaks of the Doppler background are now $\sim$ 250 MHz apart. This shifts the zero-crossing frequency of the $F = 2 \rightarrow F' = 2, 3$ crossover feature by (4.4 ± 0.1) MHz. Further reductions in polarization purity produce increasingly different spectra at successive zero-crossing angles due to the complex interplay between sub-Doppler features and the Doppler background. For very poor polarization purity ($\sim$ $15 : 1$), the sub-Doppler features are both qualitatively different in their lineshapes and located in different regions of the Doppler background, *e.g.* near the minimum as opposed to halfway up the side of the Doppler-broadened peak.

This behaviour has clear implications for laser locking. The error signals generated by such poorly linearly polarized beams will be more sensitive to small changes in polarization due to *e.g.* changes in temperature. The magnetic field dependence of the error signal's zero-crossing will also differ between zero-crossing angles, as some sub-Doppler features may be located in a flat region of the Doppler background, and

others on a slope. Polarization spectra are also sensitive to impurities in polarization, although a detailed study is beyond the scope of this work. It is therefore advisable to make the polarization purity of the system as high as is practical. Note, however, that very good purity can be achieved without recourse to (expensive) specialised optics, and improvements in polarization purity above 300-400:1 will yield diminishing returns as other factors (e.g. differences in the responsivity of the two photodiodes) can also produce a separation in zero-crossing angles.

5. Conclusions

In summary, we have studied sub-Doppler DAVLL spectra for the Rb D2 transitions. The importance of polarization purity in generating the spectra was discussed, and the dependence of the amplitude and gradient of the error signals produced were characterised as a function of magnetic field and pump power. We suggest operating parameters which maximise the signal gradient and amplitude for the ^{87}Rb $F = 2 \rightarrow F' = 3, 2$ crossover transition. A comparison with polarization spectroscopy showed similar amplitudes and gradients for the largest features of each scheme, and the reasons for specific features having different amplitudes were discussed.

Acknowledgments

This work is supported by the EPSRC. SLC acknowledges the support of the Royal Society. We thank D J McCarron for laboratory assistance, and C S Adams and M P A Jones for fruitful discussions.

References

[1] Chu S 1998 *Rev. Mod. Phys.* **70** 685; Cohen-Tannoudji C N 1998 *Rev. Mod. Phys.* **70** 707; Phillips W D 1998 *Rev. Mod. Phys.* **70** 721
[2] Rovera G D, Santarelli G and Clairon A 1994 *Rev. Sci. Instrum.* **65** 1502
[3] Bjorklund G C 1980 *Opt. Lett.* **5** 15
[4] Wieman C and Hänsch T W 1976 *Phys. Rev. Lett.* **36** 1170; Pearman C P, Adams C S, Cox S G, Griffin P F, Smith D A and Hughes I G 2002 *J. Phys. B* **35** 5141; Ratnapala A, Vale C J, White A G, Harvey M D, Heckenberg N R and Rubinsztein-Dunlop H 2004 *Opt. Lett.* **29** 2704
[5] Chéron B, Gilles H, Hamel J, Moreau O and Sorel H 1994 *J. de Physique III* **4** 401; Corwin K L, Lu Z-T, Hand C F, Epstein R J, and Wieman C E 1998 *Appl. Opt.* **37** 3295; Millett-Sikking A, Hughes I G, Tierney P and Cornish S L 2007 *J. Phys. B* **40** 187
[6] Petelski T, Fattori M, Lamporesi G, Stuhler J and Tino G M 2002 *Eur. Phys. J. D* **22** 279
[7] Wasik G, Gawlik W, Zachorowski J and Zawadzki W 2002 *Appl. Phys. B* **75** 613
[8] Robins N P, Slagmolen B J J, Shaddock D A, Close J D and Gray M B 2002 *Opt. Lett.* **27** 1905; Jundt G, Purves G T, Adams C S and Hughes I G 2003 *Eur. Phys. J. D* **27** 273
[9] Gilles H, Cheron B and Hamel J 2001 *Opt. Comm.* **190** 179; Purves G T, Jundt G, Adams C S and Hughes I G 2004 *Eur. Phys. J. D* **29** 433
[10] Sukenik C I, Busch H C and Shiddiq M 2002 *Opt. Comm.* **203** 133; van Ooijen E D, Katgert G and van der Straten P 2004 *Appl. Phys. B* **79** 57
[11] Kerckhoff J A, Bruzewicz C D, Uhl R and Majumder P K 2005 *Rev. Sci. Inst.* **76** 093108

[12] Park S E, Lee H S, Kwon T Y, Cho H 2001 *Opt. Comm.* **192** 49
[13] Tiwari V B, Singh S, Mishra S R, Rawat H S and Mehendale S C 2006 *Opt. Comm.* **263** 249; Tiwari V B, Singh S, Mishra S R, Rawat H S and Mehendale S C 2006 *Appl. Phys. B* **83** 93
[14] MacAdam K B, Steinbach A and Wieman C 1992 *Am. J. Phys.* **60** 1098; Smith D A and Hughes I G 2004 *Am. J. Phys.* **72** 631
[15] Maguire L P, van Bijnen R M W, Mese E and Scholten R E 2006 *J. Phys. B* **39** 2709; Moon G and Noh H R 2007 *J. Korean Phys. Soc.* **50** 1037
[16] Arimondo E, Inguscio M and Violino P 1977 *Rev. Mod. Phys.* **49** 31
[17] Harris M L, Adams C S, Cornish S L, McLeod I C, Tarleton E and I G Hughes 2006 *Phys. Rev. A* **73** 062509
[18] McCarron D J, Hughes I G, Tierney P and Cornish S L 2007 *Rev. Sci. Instrum.* **78** 093106
[19] Reeves J M, Garcia O and Sackett C A 2006 *Appl. Opt.* **45** 372